Rapid prototyped microvessel flow phantom for controlled investigation of ultrasound-mediated targeted drug delivery

Roger Domingo-Roca
Electronic & Electrical Engineering
University of Strathclyde
Glasgow, United Kingdom
roger.domingo-roca@strath.ac.uk

Brian Saltin
Electronic & Electrical Engineering
University of Strathclyde
Glasgow, United Kingdom
brian.saltin@strath.ac.uk

James Windmill
Electronic & Electrical Engineering
University of Strathclyde
Glasgow, United Kingdom
james.windmill@strath.ac.uk

Joseph Jackson
Electronic & Electrical Engineering
University of Strathclyde
Glasgow, United Kingdom
joseph.jackson@strath.ac.uk

Helen Mulvana
Biomedical Engineering
University of Strathclyde
Glasgow, United Kingdom
helen.mulvana@strath.ac.uk

***Abstract*— The ability to undertake controlled and accurate investigation of the complex features that determine microvasculature-fluid systems is essential in our progress towards successful clinical exploitation of ultrasound mediated targeted drug delivery (UmTDD). We present an engineered platform to enable accurate understanding of the microvascular flow characteristics capable of influencing UmTDD. We develop novel 3D-printed flow phantoms, accurately replicating real microvascular structures, and a new approach to investigating UmTDD phenomena that places microbubble-microvessel interactions at the heart of the problem. Our aim is to establish a robust, lab-based platform for controlled and systematic investigation of microvessel architectures as key determinants in UmTDD efficiency.**

Keywords—3D-Printing, microvasculature, ultrasound-mediated targeted drug delivery, microCT, phantom

I. INTRODUCTION (*HEADING 1*)

Targeted therapies that can treat diseases non-invasively, safely, and repeatably offer huge potential to reduce side effects [1], systemic toxicity [2], and improve local drug uptake [2]. Ultrasound-mediated targeted drug delivery (UmTDD) shows huge promise but clinical translation has been impeded by a lack of understanding of the mechanisms underpinning the process, with consequent unpredictable and low delivery efficiencies [3]. UmTDD uses microbubbles (μBs) to generate localised bio-effects in tissues and promote drug uptake.

Viability has been shown *in vitro* and pre-clinically in animals [2,4] across a wide range of diseases (e.g. cancer and diabetes) and drug combinations. Detailed and on-going *in vitro* studies have led to significant advances in our understanding of the possible cellular uptake mechanisms responsible for UmTDD, but it remains unclear how these are influenced by microvessel characteristics and flow conditions. The result is a weak correlative relationship between theoretical understanding, laboratory results, animal experimentation, and clinical tests.

We believe that the ability to develop better understanding of the complex microvascular-fluid system and its influence on μBs and microvessel interactions are essential to the exploitation of TDD as a clinically applicable technology.

In this work, we present the design of a new protocol for controlled and repeatable experimental investigation of UmTDD. Using porcine mesentery, we extract the structure of microvasculature using microCT and present statistical information on the geometry and structure of the blood vessels. Although based on off-the-shelf polymers, the 3D-printing materials are customised to have acoustic and mechanical properties close to real tissue in order to replicate *in vivo* systems and provide a high degree of experimental accuracy. The overall aim of this work is to provide a method in which new techniques can be rapidly prototyped and validated. We demonstrate that such systems can be used to develop a better understanding of the key parameters capable of influencing drug delivery efficiency and distribution and allow controlled investigation of deterministic variables.

II. MATERIALS AND METHODS

A. MicroCT

The geometry and structure of microvessel networks were acquired using X-ray microCT (Bruker, Skyscanner, 1172). Porcine mesentery tissue (Medical Meats, Rochdale, UK) was thawed and stained with 1% weight/volume (w/v) Iodine (I2) in absolute ethanol overnight [5] and mounted before it was scanned at 69 kV, 100 μA, and pixel size resolution of 27 microns. Rotational scanning was performed about the vertical axis with camera exposure time of 600 ms, rotation step of 0.6º, and frame averaging of 2. X-rays were filtered with a 0.5 mm thick aluminium screen. A flat-field correction was taken prior to scanning to correct for pixel sensitivity of the camera. Finally,

acquisitions were post-processed in Amira 6.3 © (Thermo Fisher Scientific, Hillsboro, OR, USA). 3D reconstruction was performed prior to volume generation by semi-manual segmentation according to X-ray density gradients. This was supported by automated interpolation between slices, followed by optimal inspection and manual amendment.

B. 3D-Printing

A stereolithography (STL) ASIGA 3D printer (Pico2HD27UV, *x* and *y* pixel resolution of 27 µm, *z* control 1 µm, and UV wavelength 385 nm) was used.

All 3D-printed microchannels were created using a resin comprising a base monomer material, a photoinitiator, and an ultraviolet (UV) light absorber to control the penetration depth of light into the material. Poly(ethylene glycol) diacrylate (MW 250. PEGDA) combined with phenylbis(2,4,6-trimethylbenzoyl) phosphine oxide (Irgacure 819) as a photoinitiator. Sudan I was used as a UV absorber in a 0.35% weight/weight (w/w) concentration, together with 1% w/w Irgacure 819 [6-8]. The resin was sonicated to ensure uniform distribution and dissolution of Sudan I and Irgacure 819 into the polymeric matrix before 3D-printing. The microchannels were 3D-printed using a layer thickness of 5 µm at 0.6 s exposure time, and 70 s burn-in exposure time. The building block was separated from the build tray height of 3 mm at 1 mm/s.

C. Acoustic Characterisation

Density, speed of sound, attenuation coefficient, and B/A nonlinear coefficient [9] were determined. All acoustic measurements were conducted in a water tank measuring 500 x 350 x 150 mm filled with outgassed water at room temperature. A single-element broadband 3.5 MHz transducer, focal length 75 mm (Videoscan V380 Panametrics-NDT, Waltham, MA, USA) operated with a 10-cycle sinusoidal pulse with PRF 10 ms and focal pressure of 0.05 MPa was used to determine acoustic attenuation. Signals were received using a calibrated needle hydrophone (Precision Acoustics, Ltd., Dorset, UK) with a 0.5 mm active tip connected to a DC coupler through a 50 Ohm connector with 6 dB damping. For speed of sound measurements, the same transducer was used in pulse-echo mode driven using a pulser-receiver (JSR Ultrasonics DPR300, Imaginant Inc., Pittsford, NY, USA). To determine B/A, two single-element planar transducers of 2 MHz and 5 MHz were driven as described above and signals received using the hydrophone.

Acoustic attenuation values (α) were determined by comparing the root-mean-square pressure amplitude in clear transmission (P_0) with that after propagation through the 3D-printed samples (P) according to (1).

$$\alpha = -20\log(P/P_0) \tag{1}$$

The speed of sound, *c*, was determined by identifying the acoustic time delay between the front and back of the 3D-printed sample observed using an oscilloscope. The nonlinear B/A coefficient was calculated using (2) [10].

The Carnegie Trust for the Universities of Scotland, Grant number 50354.

$$\beta = \beta_r \sqrt{\frac{\rho_s c_s^5 T_s^I \phi_s}{\rho_r c_r^5 T_r^I \phi_r}} \tag{2}$$

where the subscripts *r*, and *s* correspond to the reference (distilled water) and sample, respectively. ρ is the density, *c* the speed of sound, and *T* is the frequency-independent intensity transmission coefficient from the ultrasonic source into the material being measured. ϕ is the ratio between the measured signals from the transducer, given by (3).

$$\phi_i = \left. \frac{|V_{2f}(x)|^2}{x^2\left(|V_{1f}(0)|^2\right)^2} \right|_{x \to 0} \tag{3}$$

The sub-indices *1f* and *2f* refer to the fundamental and second harmonic frequencies, respectively. The coefficient β was used to calculate B/A using (4).

$$\beta = 1 + \frac{B}{2A} \tag{4}$$

Combining (2) and (4) to determine B/A, β_r of 3.6 was assumed for distilled water [11].

III. Results

Maximum and minimum internal vessel diameters of 261 µm and 139 µm, respectively, were measured. The 3D-printed structures featured internal diameters from 200 µm to 500 µm (Fig. 1A). Flow velocity and Reynolds (Re) numbers were determined to ensure experimental accuracy and accurate replication of biological flow conditions *in vivo* (Fig. 1B). The acoustic attenuation coefficient, speed of sound, and B/A nonlinear coefficient of the 3D-printed material were fully characterized (c = 1114 m/s, ρ = 1243 kg/m^3, and average B/A coefficient of 6.07).

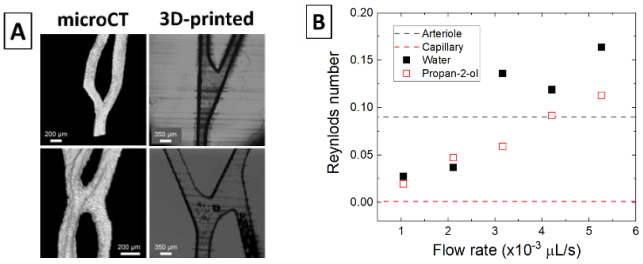

Fig. 1. (A) Comparison betwenn microCT scans of a vessel network and the fluid-filled 3D-printed microchannels. (B) Shows the Reynolds (Re) numbers measured within a 3D-printed PEGDA microchannel as a function of flow rate (in µL/s). The red and the black dashed lines represent, respectively, the Re numbers obserd in arterioles and capillaries.

A. X-ray microCT scans

Software reconstruction of the scanned sample was performed using NRecon (Bruker Corporation, Billerica, MA, USA). A smoothing factor 1 (in a scale from 0 to 10) was applied to the processed faces, a ring artefact correction factor of 14, and beam hardening correction factor of 49%. A primary clean-up based on speckle removal was performed with CTan software (Bruker Corporation, Billerica, MA, USA) using a thresholding intensity of 27-255. Sweeping was applied to all except the largest object in the 3D space, as reported by Alba-Tacedor [12].

A representative reconstructed X-ray scan of the vessel networks found in the porcine mesentery samples is shown in Fig. 2A. Fig. 2B highlights the potential regions of interest for UmTDD.

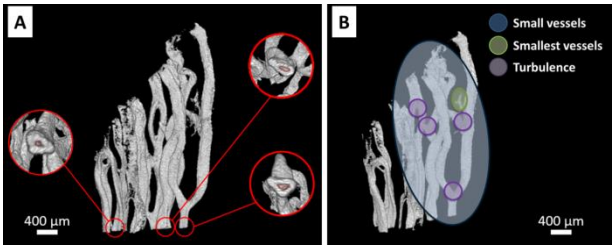

Fig. 2. Post-processed X-ray microCT image of one of the pig mesentery samples. (A) The vessel network presents a three-dimensional geometry. The red circles show magnified views of representative vessel cross-sections. This data was used to determine diameter. (B) The model allows relevant morphological sites of interest to be readily interrogated.

The information obtained from microCT scans permits to produce 3D models of vessel networks for rapid prototyping of flow phantoms.

B. 3D-printed microchannels

Microchannels consisting of an inlet and two outlets were 3D-printed. The average microchannel width of the inlet and two outlets (± s.e.) was 189 ± 3 µm, 158 ± 4 µm, and 158 ± 3 µm, respectively, with expected width of 200 µm. Unobstructed flow through the printed channels was observed in 31 % of them. When printing 500 µm (expected) width, the measured average widths (± s.e.) were 502 ± µm, 478 ± 2 µm, and 478 ± 3 µm for the inlet and the two outlets, respectively. Unobstructed flow was observed in 90% of the printed microchannels.

As the features of interest become smaller, higher deviation from the expected dimensions is observed because of the resolution limits of the 3D printer. Nevertheless, knowing the relationship between the expected and the experimental dimensions, it is possible to establish a compensation factor that allows for accurate replication of real dimensions.

C. Fluid flow analysis

A syringe pump (Cole-Parmer, Eaton Socon, UK) was connected to the inlet of the 3D-printed microchannels using butterfly needles (Medisave, Dorset, UK), with outlets open to atmospheric pressure. Vessels were purged prior to commencing any experiment to ensure that air bubbles were not introduced. Flow velocity and Re numbers were established and used to ensure that experimental parameters accurately replicate various biological flow conditions *in vivo* of interest for investigation.

Table I demonstrates that our approach can be used to successfully reproduce Re numbers similar to those observed in the arterioles and capillaries of the human body. Water was first chosen to replicate the Re numbers observed in real vessel networks by changing the flow rate (in µL/s) delivered by the syringe pump. Given the steep increase observed when using water with flow rate, propan-2-ol was used as a second study fluid.

TABLE I. VELOCITY AND REYNOLDS NUMBER, RE, MEASURED IN REAL HUMAN VESSELS AND IN OUR 3D-PRINTED SYSTEMS.

In human body [20]		
Vessel	***Peak velocity (m/s)***	***Re number (peak)***
Arteriole	$5 \cdot 10^{-3} – 1 \cdot 10^{-2}$	0.09
Capillary	$2 \cdot 10^{-4} – 1.7 \cdot 10^{-3}$	0.001

Measured in phantom			
Liquid	***Flow rate (10^{-3} µL/s)***	***Velocity (mm/s)***	***Re number***
Water	5	0.33	0.16
	4	0.24	0.12
	3	0.27	0.14
	2	0.07	0.04
	1	0.06	0.03
Propan-2-ol	5	0.41	0.11
	4	0.34	0.09
	3	0.22	0.06
	2	0.17	0.05
	1	0.07	0.02

This study provides the materials and settings required to faithfully reproduce fluid behaviours as observed in vessel networks *in vivo*.

D. Acoustic characterization

Density, speed of sound, attenuation coefficient, and B/A coefficient of PEGDA were measured to assess its ability to replicate the acoustic properties of human tissue.

The average PEGDA density (± s.e.) of 1243 ± 30 kg/m^3. This value allowed to calculate speed of sound (c) using (5), where the isentropic bulk modulus, K, is used. K can be related to the elastic modulus, E (0.9 GPa), and the Poisson's ratio, υ (0.35) [21], of the material.

$$c = \sqrt{K/\rho} = \sqrt{E/3\rho(1-2\upsilon)} \quad (5)$$

Equation (5) leads to a theoretical c of 897 ± 68 m/s. This value can be experimentally verified using the experimental set up described in the Materials and Methods Section, obtaining an average value of 966 ± 31 m/s.

The attenuation coefficient, α, is presented in Fig. 3.

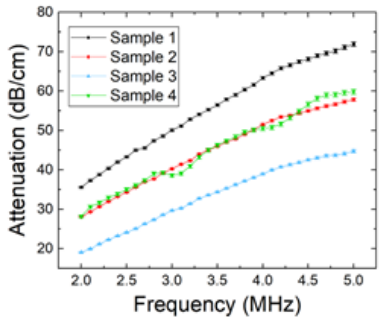

Fig. 3. Attenuation coefficient, α, of 4 different 3D-printed PEGDA samples.

Finally, the B/A of the 3D-printed material was determined and compared to values for biological materials. (Table II).

TABLE II. B/A OF THE 3D-PRINTED MATERIAL. VALUES FOR GLYCEROL AND SEVERAL BIOLOGICAL MEDIA ARE PROVIDED FOR COMPARISON.

	Literature	***Experimental data***		***Experimental data***
Glycerol [13]	9.2	9.7	Sample 1	3.7
Beef liver [13]	7.7	-	Sample 2	4.6
Beef brain [13]	7.6	-	Sample 3	10.9
Beef heart [13]	7.1	-	Sample 4	2.2
Pig muscle [13]	7.8	-	Sample 5	10.0
Pig fatty muscle [13]	11.2	-	Sample 6	51.8
Fat [14]	6.1	-	Sample 7	8.5
Heart [14]	3.9	-	Sample 8	2.6
Muscle [14]	4.7	-		

The experimental method to measure B/A was validated with a well characterised control sample (glycerol). The resulting variability is hypothesized to result from the amorphous polymer structure of the samples, and non-uniformity of the 3D-printed layers. Nevertheless, the measured B/A values indicate that PEGDA will have similar nonlinear effect on the propagating sound waves as tissue. It can be further observed that even within the literature, measured B/A values present high variability since its measurement is highly dependent on the amplitude and frequency of the interrogating sound source.

IV. CONCLUSIONS

This work presents the tools that will enable a new approach for controlled investigation of fluid flow as a parameter of relevance to understand and predict UmTDD efficiency and applicability. This innovative protocol, which minimises animal use by introducing 3D-printing technology, provides a platform that will allow investigation of the geometric features of the microvasculature capable of influencing fluid flow and, consequently, transport of systemically circulating particles such as microbubbles.

The ability to accurately replicate microvessel networks will be essential to further our collective understanding of the physical phenomena underpinning UmTDD, with particular emphasis on the ability to predict where and when it can occur. We present a protocol to rapidly prototype structure of potential influence in UmTDD to support their controlled investigation.

Fluid dynamics in the 3D-printed microchannels have been shown to faithfully reproduce the fluidic conditions observed in the human body. Furthermore, the acoustic properties of the 3D-printed phantoms were studied. While the speed of sound and the attenuation coefficient are slightly lower and higher, respectively, than those reported for biological media, the density and nonlinear of the 3D-printed material have been observed to match those found in biological media. These discerning properties can, nevertheless, be improved by changing the composition of the 3D-printed material.

The ability to accurately replicate microvessel networks will be essential to study the physical phenomena underpinning UmTDD efficiency and applicability. This work provides a platform to rapidly prototype any structure that is suspected to play a key role in UmTDD treatments.

ACKNOWLEDGMENT

The authors would like to thank Dr. Richard O'Leary for technical discussion and equipment support.

REFERENCES

[1] H. Wang, et al., "Nanoparticle systems reduce systemic toxicity in cancer treatment", Nanomedicine, vol. 11, pp. 103–106, 2015.

[2] J. L. Dembinski, et al., "Reduction of nontarget infection and systemic toxicity by targeted delivery of conditionally replicating viruses transported in mesenchymal stem cells", Cancer Gene Ther., vol. 17, pp. 289-297, 2010.

[3] S. Hernot, and A. L. Klibanov, "Microbubbles in ultrasound-triggered drug and gene delivery", Adv. Drug Deliv. Rev., vol. 60, pp. 1153–1166, 2008.

[4] G. Lajoine, et al., "In vitro methods to study bubble–cell interactions: Fundamentals and therapeutic applications" Biomicrofluidics, vol. 10, 011501, 2016.

[5] C. M. H. Newman, and T. Bettinger, "Gene therapy progress and prospects: ultrasound for gene transfer" Gene Therapy, vol. 14, pp. 465–475, 2007.

[6] B. D. Metscher, "MicroCT for comparative morphology: simple staining methods allow high–contrast 3D imaging of diverse non-mineralized animal tissues" BMC Physiol., vol.9, pp. 11–24, 2009.

[7] B. Tiller, et al., "Piezoelectric Microphone via Digital Light Processing 3D Printing Process" Mater. Des., vol. 165, 107593, 2019.

[8] R. Domingo-Roca, et al., "Bio-inspired 3D-printed piezoelectric device for acoustic frequency selection" Sensor. Actuat. A–Phys., vol. 271, pp. 1–8, 2018.

[9] H. Gong, et al., "Optical approach to resin formulation for 3D printed microfluidics" RSC Adv., vol. 5, pp. 106621–106632, 2015.

[10] B. Zeqiri, et al., "On measurement of the acoustic nonlinearity parameter using the finite amplitude insertion substitution (FAIS) technique" Metrologia, vol. 52, pp. 406-422, 2015.

[11] K. D. Wallace, et al., "Finite amplitude measurements of the nonlinear parameter B/A for liquid mixtures spanning a range relevant to tissue harmonic mode" Ultrasound Med. Biol., vol. 33, pp. 620–629, 2010.

[12] J. Alba-Tacedor, "From the sample preparation to the volume rendering images of small animals: a step by step example of a procedure to carry out the micro-CT study of the leafhopper insect *Homoalodisca vitripennis* (Hemiptera: Cicadellidae)" Proceedings of the Bruker micro-CT User Meeting, Ostende, pp. 260-288, 2014.

[13] W. K. Law, et al., "Determination of the nonlinearity parameter B/A of biological media" Ultrasound Med. Biol., vol. 11, pp. 307–318, 1985.

[14] R. van Sloun, et al., "Ultrasound coefficient of nonlinearity imaging" IEEE Trans. Ultrason. Ferroelectr. Freq. Control, vol. 62, pp. 1331–1341, 2015.